Catalysis Today 180 (2012) 184–189

Contents lists available at SciVerse ScienceDirect

Catalysis Today

journal homepage: www.elsevier.com/locate/cattod

Effect of different alumina dopants on the redox deactivation produced by structural modifications on $CePrO_x/Al_2O_3$ systems

Ginesa Blanco[a], José María Pintado[a,*], Karima Aboussaïd[a,b], Gustavo Aurelio Cifredo[a], Mohamed Soussi el Begrani[b], Serafín Bernal[a]

[a] Departamento de Ciencia de los Materiales e Ingeniería Metalúrgica y Química Inorgánica, University of Cádiz, Apdo. 40, Puerto Real (Cádiz) 11510, Spain
[b] Département de Chimie, Equipe de Catalyse Environnementale, Faculté des Science, Université Abdelmalek Essaadi, B.P. 2121 Mhannech II, 93002-Tétouan, Morocco

ARTICLE INFO

Article history:
Received 10 February 2011
Received in revised form 30 August 2011
Accepted 24 September 2011
Available online 6 November 2011

Keywords:
Ce/Pr mixed oxide
Alumina-supported catalysts
OSC
Thermal aging
Redox behaviour, FTIR spectroscopy

ABSTRACT

Two alumina-supported Ce/Pr mixed oxides, with different alumina promoters, La and Si, have been investigated in this paper. A gradual decrease of the Oxygen Storage Capacity (OSC) was observed after reducing the samples at progressively higher temperatures. However, depending on the nature of the alumina promoter, the temperature at which the loss of OSC started to be evident changed, being higher in the La-doped sample. A structural characterization study by X-ray diffraction (XRD) of the samples submitted to different reduction and reoxidation treatments in a range of temperatures was performed. From this study a correlation between the nature of the observed phases, the alumina promoter, and the deactivation behaviour could be stated. FTIR study is of particular interest because the observed correlation between the reduction degree and the position and intensity of the FTIR band is altered when deactivation phenomena appear.

1. Introduction

Ceria-based materials as well as related metal-supported systems, including alumina-supported ceria-based mixed oxides, are widely used in catalytic applications [1–4], such as in three way catalysts, methane and other hydrocarbons combustion, syngas generation from hydrocarbons, or generation of new fuels such as hydrogen or biodiesel.

It is well known that the ability for an efficient oxygen exchange with the surrounding environment plays a key role in the catalytic applications of this kind of materials [5–9]. Ce/Pr mixed oxides have shown to improve the oxygen exchange properties with respect to pure ceria [9–12].

The loss of this property in ceria-based materials is a major cause of deactivation. In alumina supported mixed oxides, redox deactivation can be attributed to the incorporation of reduced trivalent cations in the structure of alumina [13,14]. This effect causes the formation of an aluminate with perovskite-like structure, being thus stabilized the reduced trivalent cations and their oxidation to the tetravalent oxidation state is avoided. A loss in their ability to exchange oxygen, and the subsequent redox deactivation is inherent to this process.

Two different alumina-supported mixed oxide systems, where the nature of the dopant included to stabilize the alumina was changed (Si or La) have been investigated, and their redox and structural properties compared. The existence of Ce^{3+} in reduced samples can be revealed by an electronic transition characteristic of this cation, which can be observed in the infrared region, and thus followed by FTIR spectroscopy. This electronic transition has been reported by Lavalley et al. in [15], and has been used later in studies on the reduction processes undergone by ceria-based mixed oxides [16].

In this work, deactivation in alumina-supported lanthanide mixed oxides has been studied by DRX and OSC measurements combined with the study by FTIR of the evolution of the electronic transition absorption band attributed to Ce^{3+}. The correlation between the results obtained by the different techniques mentioned above allows us using FTIR spectroscopy as a tool for monitoring redox deactivation effects undergone by alumina-supported ceria-based mixed oxides.

From this work, it has been shown that the different nature of the dopant plays a key role in the redox deactivation phenomena.

2. Experimental

In this paper, two alumina-supported Ce/Pr mixed oxide systems have been investigated. The silica- and lanthana-modified aluminas used as support were kindly provided by Grace. Silica and lanthana loadings were 3.5 wt% and 4 wt%, respectively.

* Corresponding author. Tel.: +34 956016345; fax: +34 956016337.
E-mail address: josemaria.pintado@uca.es (J.M. Pintado).

0920-5861/$ – see front matter © 2011 Elsevier B.V. All rights reserved.
doi:10.1016/j.cattod.2011.09.039

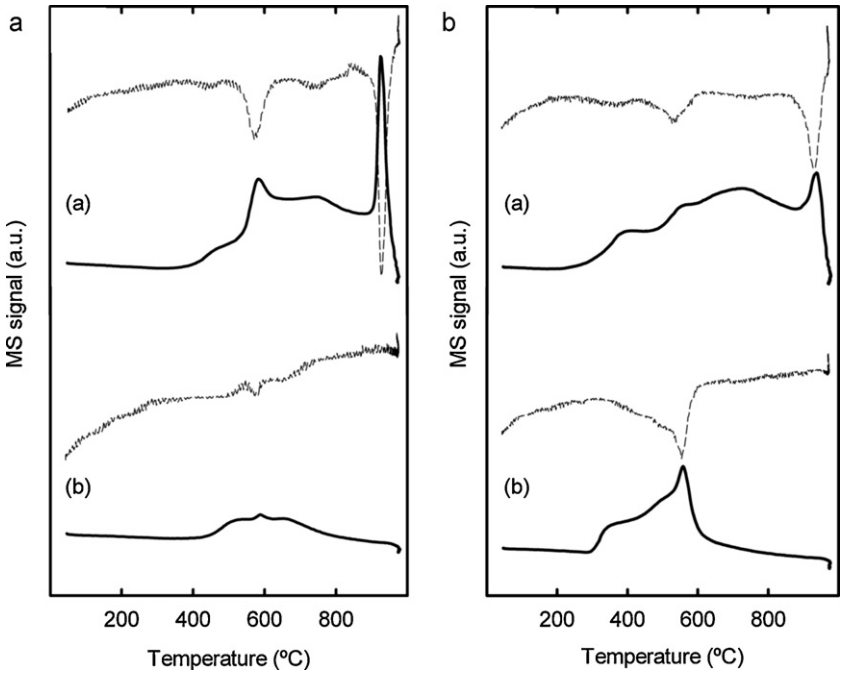

Fig. 1. TPR-MS profiles of the alumina supported Ce/Pr mixed oxydes: (A) P20C/Al_2O_3–La_2O_3; (B) P20C/Al_2O_3–SiO_2. Traces (a) correspond to the first TPR, and traces (b) to a second successive TPR. Solid lines represent water evolution, m/c:18, and dotted lines correspond to hydrogen consumption, m/c:2.

A Ce/Pr mixed oxide, with a molar ratio Ce:Pr 80:20, was deposited over each alumina by incipient wetness impregnation with an aqueous solution of the corresponding nitrates. The mixed oxide loading was set to 25 wt% on the alumina. The final compositions of the samples were: 25% $Ce_{0.8}Pr_{0.2}O_{2-x}$/Al_2O_3–SiO_2 and 25% $Ce_{0.8}Pr_{0.2}O_{2-x}$/Al_2O_3–La_2O_3, and will be referred to as P20C/Al_2O_3–Si and P20C/Al_2O_3–La, respectively. Finally, the impregnated samples were dried, calcined in air at 500 °C, and stored, being their BET surface area 157 and 142 m^2/g for the silica- and lanthana-loaded samples, respectively.

Temperature programmed reduction (TPR) studies were performed on an experimental setup coupled to a Pfeiffer quadrupole mass spectrometer (MS). The device was equipped with mass flow controllers and electronic control of the oven temperature. The TPR-MS runs were performed under the following conditions: amount of sample: 200 mg, H_2(5%)/Ar flow rate: 60 cm^3/min, heating ramp: 10 °C/min. Prior running the experiments, the samples were submitted to a pretreatment consisting on oxidation under 60 mL/min of O_2(5%)/He at 500 °C for 1 h, and cooling to room temperature.

Oxygen storage capacity (OSC) was measured by oxygen consumption at 200 °C in a Micromeritics ASAP-2020 volumetric adsorption device. Prior to the OSC measurements, the samples were reduced for 1 h under H_2(5%)/Ar flowing at 60 mL/min, at a selected temperature, ranging from 500 to 900 °C. After the reduction, the samples were evacuated to remove adsorbed H_2, for 1 h at the same reduction temperature. After reduction at 900 °C, still more than 80% of the surface area was retained by the samples, being BET surface area 127 m^2/g for P20C/Al_2O_3-Si, and 117 m^2/g for P20C/Al_2O_3-La.

X-ray powder diffraction (XRD) studies were carried out on a Bruker instrument, model D8 Advance (radius 250 mm). The diffractograms were recorded using Cu-Kα radiation (1.5406 Å) and a scan range from 13° up to 145°.

For the IR studies samples were pressed into a self supported disk (ca. 10 mg cm^{-2}). All the reduction and evacuation processes were performed *in situ* in a quartz cell. Spectra were recorded at room temperature in the transmission mode on a Bruker, Vertex 70, instrument.

3. Results and discussion

3.1. Redox characterization

The reduction behaviour of the alumina-supported Ce/Pr oxides was first investigated by means of the TPR technique. Fig. 1 shows TPR-MS diagrams corresponding to P20C/Al_2O_3–La_2O_3 (a) and P20C/Al_2O_3–SiO_2 (b) systems after the cleaning pretreatment described in Section 2 (a-traces). Water evolution and H_2 consumption are plotted on the figure. During the TPR experiment, both reduction of the supported mixed oxide (observed as H_2 consumption accompanied by water evolution), and alumina dehydroxylation occur along a wide temperature range. After the corresponding TPR experiments, the samples were kept 1 h at 900 °C under flowing H_2/Ar, then evacuated at the same temperature for an additional hour, and cooled down to room temperature. Finally, they were reoxidized at 500 °C under a flow of O_2(5%)/He. Then, a second TPR was run (traces labelled as b in Fig. 1). A dramatic effect on the reduction process was observed in this second run, both H_2 consumption and water evolution were strongly affected, indicating that little reduction has occurred during this second TPR experiment. Also worth of noting is the difference between the two samples investigated. While almost no reduction is observed for the lanthana-modified system, the silica-containing sample still shows significant reduction, although it is less important than in the first run.

Oxygen storage capacity was evaluated at temperatures above 500 °C (Fig. 2), as according to the TPR traces, the reduction degrees of the samples should be significantly high. As expected, OSC increases with the temperature when the samples are reduced up to 800 °C. At 900 °C, the oxygen consumption of the reduced sample decreases strongly, in good agreement with that observed for the TPR experiments in Fig. 1. In the case of P20C/Al_2O_3–La_2O_3, the measured OSC after reduction at 900 °C is negligible, while for

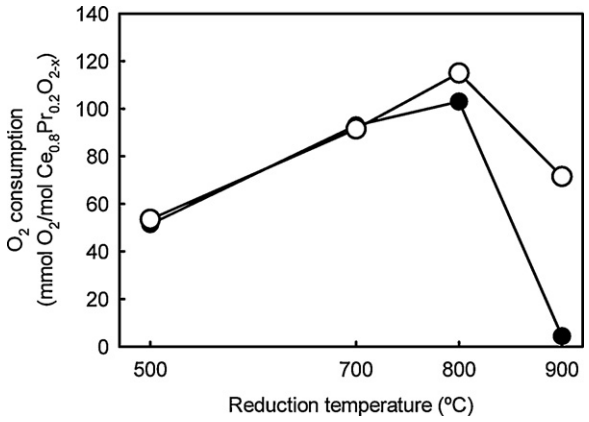

Fig. 2. Oxygen storage capacity of the Si (open circles) and La-doped samples (solid circles).

P20C/Al_2O_3–SiO_2, although there is a strong decrease, the sample still retains some OSC.

TPR experiments in Fig. 1, and OSC measurements in Fig. 2, show complementary aspects of the reduction process in these samples. While the TPR technique shows how the reduction is progressing, an OSC measurement accounts for the oxygen that a pre-reduced sample is able to uptake to completely reoxidize. The first runs for the TPR experiments showed that reduction of the samples proceeded, but the low OSC values measured after reducing at 900 °C indicate that the reoxidation process is somehow blocked.

3.2. Structural characterization

Structural changes undergone by the samples during the reduction treatments were followed by X-ray diffraction. XRD diagrams of as prepared samples (Fig. 3) were very similar, being dominated by the mixed oxide fluorite-like phase peaks, with average crystal sizes around 8–9 nm. Although less intense, peaks corresponding to the alumina support could also be observed.

The samples were reduced at 700 °C, 800 °C or 900 °C. After reduction, a careful protocol was followed, consisting on cooling down the samples at −90 °C under flowing He, switching to O_2(5%)/He at the same temperature, and slowly warming up to room temperature. This passivation protocol was employed to avoid fast and uncontrolled reoxidation of the reduced samples by sudden contact with air during their transport to the X-ray diffractometer.

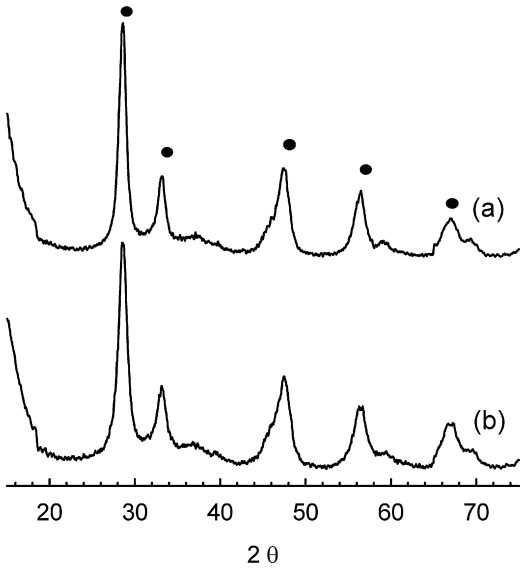

Fig. 3. X-ray diffraction patterns corresponding to: (a) P20C/Al_2O_3–La_2O_3; and (b) P20C/Al_2O_3–SiO_2. Peaks corresponding to fluorite structure are identified by the solid circles.

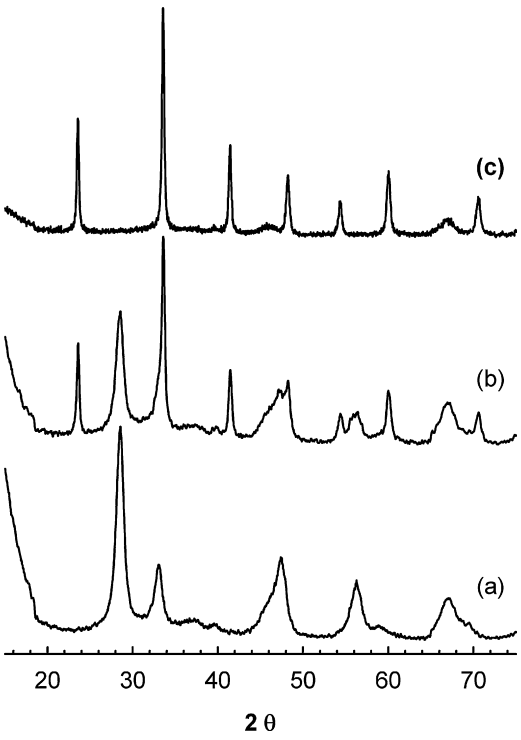

Fig. 4. X-ray diffraction patterns corresponding to P20C/Al_2O_3–La_2O_3 reduced at 700 °C (a), 800 °C (b) and 900 °C (c), and passivated prior atmospheric exposure as described in the text.

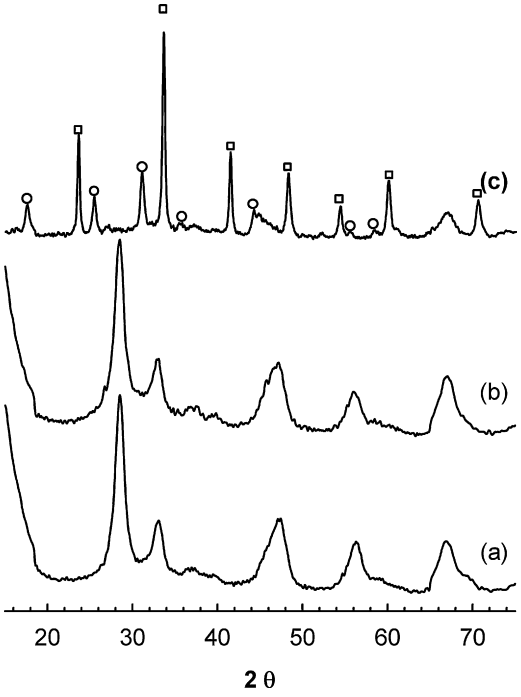

Fig. 5. X-ray diffraction patterns corresponding to P20C/Al_2O_3–SiO_2 reduced at 700 °C (a), 800 °C (b) and 900 °C (c), and passivated prior atmospheric exposure as described in the text. Hollow squares identify peaks corresponding to the perovskite structure, circles point to bastnesite structure peaks.

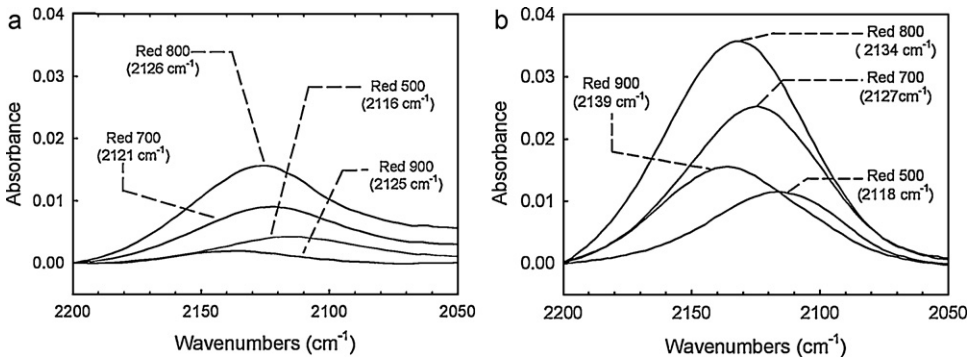

Fig. 6. *In situ* FTIR spectra of P20C/Al_2O_3–La_2O_3 (a) and P20C/Al_2O_3–SiO_2 (b) reduced at the indicated temperatures.

Fig. 4 shows the corresponding diffractograms for La-doped sample. As it can be seen from the figure, after reducing at 700 °C there are no structural changes that could be detected by XRD. When the sample is reduced at 800 °C, peaks corresponding to a new phase appear, added to those of the fluorite and alumina structures. This new peaks evidence the formation of bigger crystals (about 30 nm) of a lanthanide aluminate ($LnAlO_3$, Ln = La^{3+}, Pr^{3+}, Ce^{3+}), with a perovskite-type structure. Finally, after reduction at 900 °C, no evidence of fluorite phase can be found in the diagram, being the diffractogram dominated by the perovskite-type phase. The structural evolution of this sample can be easily related to its redox behaviour. In Fig. 2, the dramatic decrease of OSC that occurs after reducing at 900 °C, can be related to the formation of the lanthanide aluminate phase. This phase is known to be quite stable, being thus responsible of the deactivation detected in this sample. From the XRD study it can also be noted that the formation of the aluminate is already important after reduction at 800 °C.

A different behaviour can be found in the case of the Si-doped sample (Fig. 5). In this case, no evidence of the perovskite phase can be found after reduction at 800 °C. This structural difference between Si- and La-doped samples after reduction at this temperature, could explain the different OSC values shown by the samples. The diffractogram of the sample reduced at 800 °C is almost identical to that of the sample reduced at 700 °C (and to that of the fresh sample in Fig. 3), consisting only of fluorite and alumina structures. When comparing with the La-doped sample, it can be seen that the Si-doped system exhibits a higher resistance to deactivation by formation of the lanthanide aluminate. This structural study, thus, show that the lanthanide cations remain in the fluorite structure of Si-doped alumina supported P20C, under harder conditions than in the case of P20C/Al_2O_3–La_2O_3.

After reduction at 900 °C, Si-doped sample show evidences of the formation of the lanthanide aluminate, together with a new phase, that could be identified as a bastnesite-type structure, i.e., a lanthanide hydroxycarbonate. Average crystal sizes were 25 nm for the aluminate, and about 19 nm for the bastnesite-like crystallites. This latter phase can be formed by reaction with water and CO_2 of a heavily reduced lanthanide oxide, probably a sesquioxide with hexagonal structure ($CePrO_x$, $x \sim 1.5$). This reaction could occur after exposing to the atmosphere the reduced sample, although it can be possible that small traces of water and/or CO_2 in the He or O_2/He feedstream, passing through the sample for an extended period of time, could also be responsible of this reaction.

3.3. FTIR spectroscopy study of redox deactivation phenomena

The deactivation phenomena described in the previous section was further investigated by infra-red spectroscopy. The study was focused on the evolution undergone by a band centred at about 2120 cm^{-1}. In the literature, this absorption band is attributed to the $^2F_{5/2} \rightarrow {}^2F_{7/2}$ electronic transition of Ce^{3+} [15]. In this way, this band can be used, in principle, as a way of monitoring Ce^{3+} content in the reduced samples.

Fig. 6 shows the evolution of the above mentioned band with the different reduction treatments applied to the La-modified (Fig. 6a) and Si-modified (Fig. 6b) samples. A clear correlation can be seen between the position of the IR band and the reduction temperature, that is to say, the reduction degree reached after the reduction process. As the reduction temperature increases, up to 800 °C, the position of the Ce^{3+} band is shifted towards higher wavenumbers. Another interesting correlation has been found between the area under the electronic transition band and the amount of oxygen in the OSC measurements (Fig. 7). However, at higher temperatures, the band area decreases, thus indicating that this area is linked to the amount of reoxidizable Ce^{3+} in the sample, that is, those Ce^{3+} cations which are not included in the perovskite-like structure. At these very high temperatures, the position of the band is further shifted towards higher wavenumbers, being this in good agreement with the higher reduction degree of the reoxidizable phase, i.e., the remaining ceria-based mixed oxide component.

3.4. Reoxidation studies of heavily reduced samples

Samples reduced at 900 °C were reoxidized at 200 °C and 500 °C, and their structural properties studied by XRD. Results are summarized in Figs. 8 and 9.

In the case of La-doped sample reduced at 900 °C (Fig. 8) X-ray diffractograms after passivation, after reoxidation at 200 °C

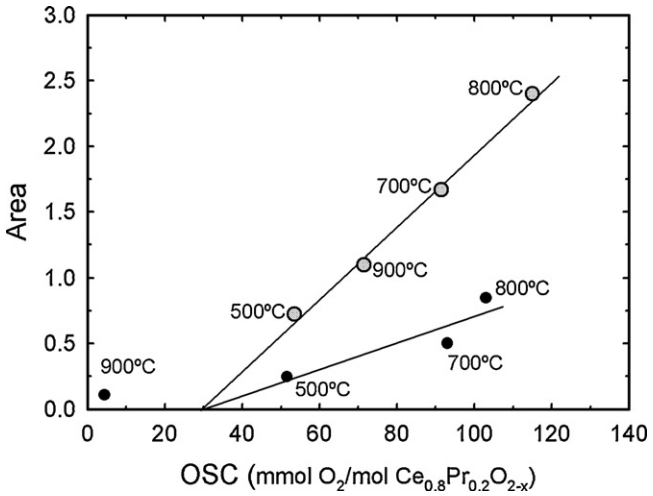

Fig. 7. Correlation between FTIR area for electronic transition band in Ce^{3+} and OSC results for P20C/Al_2O_3–La_2O_3 (solid circles) and P20C/Al_2O_3–SiO_2 (gray circles) reduced at the indicated temperatures.

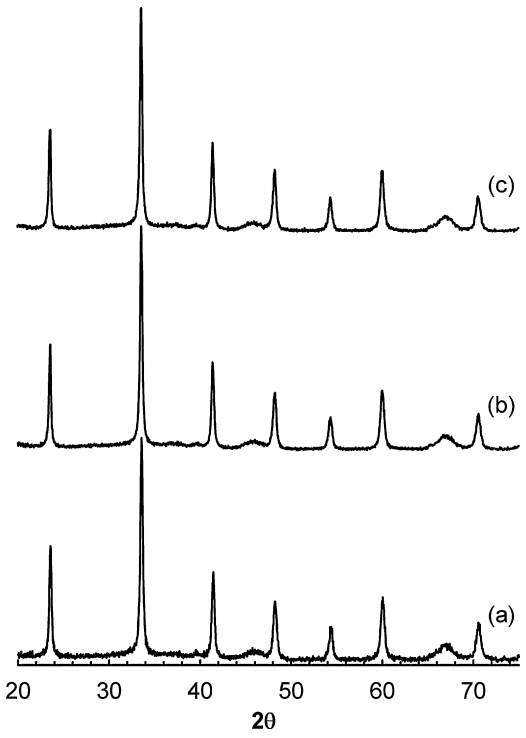

Fig. 8. X-ray diffraction patterns corresponding to P20C/Al_2O_3–La_2O_3 reduced at 900 °C and after passivation (a), reoxidation at 200 °C (b) and reoxidation at 500 °C (c).

and after reoxidation at 500 °C, are almost identical. The diagrams consist on intense and narrow peaks corresponding to the perovskite-like phase, with broader and much less intense alumina peaks. No evidence of recovery of the fluorite structure could be detected after any of the reoxidation treatments, indicating then that Ce^{3+} and Pr^{3+} cations are well stabilized in the perovskite structure.

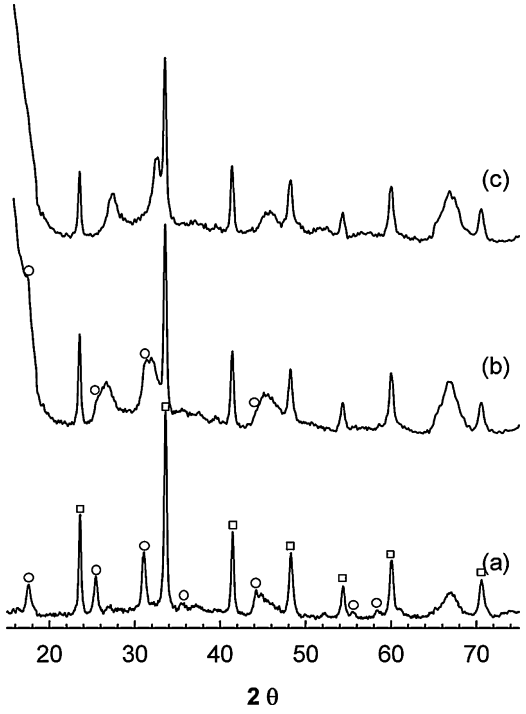

Fig. 9. X-ray diffraction patterns corresponding to P20C/Al_2O_3–SiO_2 reduced at 900 °C and after passivation (a), reoxidation at 200 °C (b) and reoxidation at 500 °C (c). Hollow squares identify peaks corresponding to the perovskite structure, circles point to bastnesite structure peaks.

The behaviour against oxidation of the heavily reduced Si-doped sample is significantly different. Fig. 9 shows the XRD data corresponding to passivation, oxidation at 200 °C and oxidation at 500 °C, of P20C/Al_2O_3–SiO_2 reduced at 900 °C. As can be seen in the figure, in contrast to the behaviour shown by the La-doped sample, further phase transformations can occur when increasing the re-oxidation temperature. These phase changes are related to the decomposition of the bastnesite phase, probably obtained by atmospheric aging of the hexagonal lanthanide sesquioxide resulting from the reduction treatment. According to the decomposition scheme proposed in [17], a lanthanide hydroxycarbonate obtained by aging the corresponding sesquioxide, with hexagonal structure, under atmospheric H_2O and CO_2, can be decomposed to the sesquioxide when heated at a temperature ranging from 450 °C and 630 °C. The decomposition, however, can start at lower temperature, passing through different intermediate phases, such as dioxymonocarbonate, or oxohydroxide phases.

Reoxidation at 200 °C of the reduced Si-doped sample (Fig. 9(b)) starts to decompose the hydroxycarbonate phase, as deduced from the broadening of the bastnesite peaks in the diffractogram. In that sense, the disappearance of the bastnesite peaks is coupled with the appearance of new peaks, shifted at higher 2θ values, so that when the sample is reoxidized at 500 °C, the bastnesite has completely disappeared, and peaks corresponding to the dioxymonocarbonate phase can be identified.

4. Conclusions

The different structural changes occurring during the reduction of two different ceria-based mixed oxides supported on modified aluminas has been investigated. Depending on the alumina modifier tested, lanthanum or silicon, both the temperature ranges where some phases start to be stable, and the nature of the identified phases, change. In this sense, when lanthanum is used to stabilize the alumina, the unwanted perovskite-like phase, $LnAlO_3$, appears at lower temperature than for Si-doped sample. This phase, which is very stable, is responsible of the redox deactivation of the supported mixed oxide, blocking its redox properties by fixing the reducible Ce and Pr ions in the +3 oxidation state. When silicon is used as alumina modifier, the perovskite phase appears at higher temperatures, providing thus a wider temperature interval for the redox activity of the sample.

The area under the Ce^{3+}electronic transition band is proportional to the amount of Ce^{3+} that can be reoxidized during the OSC experiments, that is, with the amount of Ce^{3+} non-blocked in the perovskite-type structure. On the other hand, the position of the band is related to the reduction degree of the mixed oxide, being shifted towards higher wavenumbers as its reduction degree increases. The disagreement between these parameters, i.e., the area of the IR band and the shift of the maximum, gives us information about the redox deactivation phenomena related to the blockade of Ce^{3+} cations into a perovskite-like structure.

In this context, FTIR spectroscopy is revealed as a very useful way to detect this kind of redox deactivation phenomena on these alumina-supported mixed oxide samples.

The results presented in this paper are also indicative of the strong effect that the modification of a single, minor component, in such complex systems as the ones studied here, can have a strong effect on their global behaviour.

Acknowledgements

This work has received financial support from the *Junta de Andalucía* (Group FQM 110), and the Ministry of Science and Innovation of Spain (Project MAT2008-00889-NAN). The XRD experimental studies were carried out at the corresponding facilities of the University of Cádiz.

References

[1] A. Trovarelli (Ed.), Catalysis by Ceria and Related Materials, 1st edition, Imperial College Press, London, 2002.
[2] A. Martínez-Arias, M. Fernández-García, L.N. Salamanca, R. Valenzuela, J.C. Conesa, J. Soria, J. Phys. Chem. B 104 (2000) 4038–4046.
[3] A.C.S.F. Santos, S. Damyanova, G.N.R. Teixeira, L.V. Mattos, F.B. Noronha, F.B. Passos, J.M.C. Bueno, Appl. Catal., A: Gen. 290 (2005) 123–132.
[4] L.S.F. Feio, C.E. Hori, S. Damyanova, F.B. Noronha, W.H. Casinelli, C.M.P. Marques, J.M.C. Bueno, Appl. Catal., A: Gen. 316 (2007) 107–116.
[5] G.S. Zafiris, R.J. Gorte, J. Catal. 143 (1993) 86–91.
[6] T. Bunlesin, E.S. Putna, R.J. Gorte, Catal. Lett. 41 (1996) 1–5.
[7] S. Colussi, C. de Leitemburg, G. Dolcetti, A. Trovarelli, J. Alloys Compd. 374 (2004) 387–392.
[8] S. Wang, G.Q. Lu, Appl. Catal. B: Environ. 19 (1998) 267–277.
[9] S. Bernal, G. Blanco, M.A. Cauqui, A. Martin, J.M. Pintado, A. Galtayries, R. Sporken, Surf. Interface Anal. 30 (2000) 85–89.
[10] Z.C. Kang, L. Eyring, J. Solid State Chem. 155 (2000) 129–137.
[11] C.K. Narula, L.P. Haack, W. Chun, H.W. Jen, G.W. Graham, J. Phys. Chem. B 103 (1999) 3634–3639.
[12] S. Rossignol, F. Gérard, D. Mesnard, C. Kappenstein, D. Duprez, J. Mater. Chem. 12 (2003) 3017–3020.
[13] T. Miki, T. Ogawa, M. Haneda, N. Kakuta, A. Ueno, S. Tateishi, S. Matsuura, M. Sato, J. Phys. Chem. 94 (1990) 6464–6467.
[14] J.Z. Shyu, W.H. Weber, H.S. Gandhi, J. Phys. Chem. 92 (1988) 4964–4970.
[15] C. Binet, A. Badri, J.C. Lavalley, J. Phys. Chem. 98 (1994) 6392–6398.
[16] F.C. Gennari, T. Montini, N. Hickey, P. Fornasiero, M. Graziani, Appl. Surf. Sci. 252 (2006) 8456–8465.
[17] S. Bernal, F.J. Botana, R. García, J.M. Rodríguez-Izquierdo, React. Sol. 4 (1987) 23–40.